Received: 11 December 2023 | Revised: 7 February 2024 | Accepted: 26 February 2024

DOI: 10.1002/alz.13825

Alzheimer's & Dementia®
THE JOURNAL OF THE ALZHEIMER'S ASSOCIATION

RESEARCH ARTICLE

Peripheral HMGB1 is linked to O_3 pathology of disease-associated astrocytes and amyloid

Chandrama Ahmed[1] | **Hendrik J. Greve**[1] | **Carla Garza-Lombo**[1] | **Jamie A. Malley**[1] | **James A. Johnson Jr.**[1] | **Adrian L. Oblak**[2] | **Michelle L. Block**[1]

[1]Department of Pharmacology and Toxicology, Indiana University School of Medicine, The Stark Neurosciences Research Institute, Indianapolis, Indiana, USA

[2]Department of Radiology and Imaging Sciences, Indiana University School of Medicine, The Stark Neurosciences Research Institute, Indiana University School of Medicine, Indianapolis, Indiana, USA

Correspondence
Michelle L. Block, Department of Pharmacology and Toxicology, Stark Neurosciences Research Institute, Indiana University School of Medicine, 320 West 15th Street, NB 214D, Indianapolis, IN 46202, USA.
Email: mlblock@iupui.edu

Funding information
VA Merit Award, Grant/Award Number: I01 BX004161; NIH, Grant/Award Numbers: 1RF1AG077826, RO1 ES029835GW, R01 ES028104

Abstract

INTRODUCTION: Ozone (O_3) is an air pollutant associated with Alzheimer's disease (AD) risk. The lung–brain axis is implicated in O_3-associated glial and amyloid pathobiology; however, the role of disease-associated astrocytes (DAAs) in this process remains unknown.

METHODS: The O_3-induced astrocyte phenotype was characterized in 5xFAD mice by spatial transcriptomics and proteomics. *Hmgb1*$^{fl/fl}$ *LysM*-Cre^{+} mice were used to assess the role of peripheral myeloid cell high mobility group box 1 (HMGB1).

RESULTS: O_3 increased astrocyte and plaque numbers, impeded the astrocyte proteomic response to plaque deposition, augmented the DAA transcriptional fingerprint, increased astrocyte–microglia contact, and reduced bronchoalveolar lavage immune cell HMGB1 expression in 5xFAD mice. O_3-exposed *Hmgb1*$^{fl/fl}$ *LysM*-Cre^{+} mice exhibited dysregulated DAA mRNA markers.

DISCUSSION: Astrocytes and peripheral myeloid cells are critical lung–brain axis interactors. HMGB1 loss in peripheral myeloid cells regulates the O_3-induced DAA phenotype. These findings demonstrate a mechanism and potential intervention target for air pollution–induced AD pathobiology.

KEYWORDS
amyloid plaques, disease-associated astrocytes, lung–brain axis, O_3, peripheral HMGB1

Highlights

- Astrocytes are part of the lung–brain axis, regulating how air pollution affects plaque pathology.
- Ozone (O_3) astrocyte effects are associated with increased plaques and modified by plaque localization.
- O_3 uniquely disrupts the astrocyte transcriptomic and proteomic disease-associated astrocyte (DAA) phenotype in plaque associated astrocytes (PAA).

- O_3 changes the PAA cell contact with microglia and cell–cell communication gene expression.
- Peripheral myeloid cell high mobility group box 1 regulates O_3-induced transcriptomic changes in the DAA phenotype.

1 | BACKGROUND

Alzheimer's disease (AD) is the most common neurodegenerative disease and the leading cause of dementia; however, its etiology is largely unknown, and there are few disease-modifying treatments.[1,2] Increasing evidence points to a role for environmental factors in AD risk,[3–8] with several studies implicating several components of urban air pollution in increased AD risk and cognitive deficits.[9–17] Urban air pollution is a complex mixture comprising several chemical, particulate, and gaseous components, such as ozone (O_3), which is a prevalent and chronic exposure with health effects spanning several organ systems,[18,19] including the central nervous system (CNS). In the United States, in 2022 alone, > 85 million people were exposed to air pollution levels exceeding US Environmental Protection Agency safety standards,[20] emphasizing the importance of understanding how these inhaled exposures could be affecting the brain, particularly AD pathology.

Ozone, one of the components of urban air pollution and a common ground-level air pollutant component,[19,20] increases mortality[19,21–23] with a Global Burden of Disease study attributing 12.1% of all male death in 2019 to ambient O_3 pollution along with ambient air pollution.[23] Increased temperatures catalyze ground-level O_3 accumulation;[24] thus, climate change is a concern regarding increasing O_3-associated health effects.[20] Recent epidemiology studies have implicated O_3 as a strong risk factor for cognitive decline[9,25,26] and AD risk,[27,28] with one study finding 10.4% increase in cognitive impairment risk with increased O_3.[9] Prior rodent studies support that inhalation of O_3 affects the brain, demonstrating increased oxidative stress, mitochondrial dysfunction, neuronal damage, as well memory deficits.[29–37] Increased amyloid beta (Aβ) positron emission tomography signals in response to ambient air pollution have been observed in humans;[13] however, the underlying cellular mechanisms remain unclear. O_3 is a highly reactive gas and cannot transfer to the brain after inhalation;[38–40] thus, circulating factors or trafficking peripheral immune calls have been implicated to contribute to O_3-induced CNS effects in a pathway named "the lung–brain axis,"[29,41,42], among other potential pathways.[43,44] While the majority of the inhaled O_3 reacts with the alveolar lining fluid and O_3 exposure has been extensively linked to myeloid cell infiltration in prior studies,[29] the cell-specific and peripheral mechanisms underlying the impact of O_3 on amyloid pathology are unclear.

Aβ plaque deposition is a hallmark of AD.[45–48] Astrocytes[49] and microglia[50] surround plaques to form a protective barrier, restricting plaque toxicity to the surrounding neuropil and facilitating plaque clearance.[49–55] Disease-associated astrocytes (DAAs), a recently identified reactive astrocyte subset with a unique transcriptional signature and high glial fibrillary acidic protein (GFAP) expression, surround plaques in human and 5xFAD mouse tissue.[53] We previously demonstrated that O_3 exposure impacts plaque-associated microglia in 5xFAD mice;[29] however, little is known regarding how air pollution, including O_3, affects astrocytes and their plaque microenvironment localization.

Increasing evidence suggests that peripheral and systemic immune mechanisms contribute to AD pathobiology;[29,56] for example, peripheral myeloid cells are implicated in AD and amyloid pathology.[29,57] How these cells are pathologically modified and contribute to neurological disease is unknown, but urban air pollution exposure could play a role.[29] High mobility group box 1 (HMGB1) is a ubiquitous nuclear DNA-binding chaperone actively secreted by immune and damaged cells, acting as an autocrine and paracrine signal/cytokine.[58] Importantly, circulating HMGB1 is elevated in O_3-exposed 5xFAD mice, but CNS HMGB1 expression level changes are absent.[29] Circulating HMGB1 is elevated in some AD patient populations,[59,60] implicating peripheral circulating HMGB1, but the role of HMGB1 as a transcription factor regulating specific cellular functions in AD is less known. The roles of these peripheral mechanisms in DAA phenotype development and amyloid pathology are unclear.

In the current study, we began to address these unresolved questions in the field by exploring: (1) how O_3-induced changes in the periphery may regulate the astrocyte phenotype (transcriptomic, proteomic, cell number, and cell contact) and how this is modified by localization with plaques; (2) the potential role of peripheral myeloid cells in this process; and (3) whether the loss of peripheral myeloid cell HMGB1 is linked to changes in the DAA phenotype.

2 | METHODS

2.1 | Reagents

All reagents are listed in Tables S1–S5 in supporting information.

2.2 | Animals

Male transgenic 5xFAD mice hemizygous for five familial AD mutations (APP K670N/M671L, Swedish; I716V, Florida; V717,I London; PSEN1 M146L; and PSEN1, L286V),[61]

littermate controls on a C57Bl/6J background (B6. Cg-Tg(APPSwFlLon,PSEN1*M146L*L286V)6799Vas/Mmjax; RRID: MMRRC_034848-JAX), C57BL/6J (RRID:IMSR_JAX:000664), and *LysM*-Cre (B6.129P2-Lyz2tm1(cre)Ifo/J; RRID:IMSR_JAX:004781) mice were obtained from the Jackson Laboratory. Female 5xFAD mice exhibit markedly exacerbated amyloid pathology that increases rapidly over time,[62,63] risking a ceiling effect when combined with O_3 exposure; thus, to prevent potentially confounding analyses, only male mice were used in the current study. Homozygous HMGB1 floxed (HMGB1$^{fl/fl}$) mice[64] were obtained from Riken (B6.129P2-Hmgb1 < tm1Ttg > ; BRC No. RBRC06240). *Hmgb1*$^{fl/fl}$ mice were crossed with *LysM*-Cre$^{+/+}$ mice to generate *Hmgb1*$^{fl/fl}$. *LysM*-Cre^{+} mice with deletion of HMGB1 in only peripheral myeloid cells.[29] *Hmgb1*$^{fl/fl}$. *LysM-Cre*$^{+/-}$ mice were bred to produce the experimental *Hmgb1*$^{fl/fl}$. *LysM*-Cre^{+} mice and control *Hmgb1*$^{fl/fl}$. *LysM*-Cre^{-} littermates. All *Hmgb1*$^{fl/fl}$. *LysM*-Cre mice were genotyped to confirm the presence or absence of Cre recombinase and homozygous floxed *HMGB1* alleles.

The mice were acclimated to the housing facility for at least 1 week before all studies. All mice were maintained on a 12-hour light/dark cycle (7:00 am–7:00 pm) in a specific pathogen-free environment, excluding *Helicobacter*. The complete list of pathogen exclusions is provided in Table S6 in supporting information. Experimental mice were individually housed in high-efficiency particulate-absorbing filtered ventilated polycarbonate cages with food and acidic water (pH 2.2–2.7) provided ad libitum. All experiments were completed in strict accordance with the Indiana University School of Medicine Institutional Animal Care and Use Committee protocols (29002 and 27001) and National Institutes of Health (NIH) guidelines for housing, breeding, and experimental use. All mice were treated humanely to alleviate suffering.

2.3 | O_3 exposure

Mice were exposed to O_3 in full-body Hinners inhalation chambers[65] as previously described.[29] Briefly, O_3 was produced with an HFL-10 O_3 generator (Ozonology). The O_3 concentration was continuously monitored using an ultraviolet photometric O_3 analyzer (465L, Teledyne API), and the temperature was maintained at 21 ± 2°C. Rodents have lower sensitivity to O_3 toxicity than primates[66,67] due to their complex nasal turbinates, lung morphological differences, and unique airway surfactant.[67,68] Thus, increasing exposure by a factor of three is traditionally accepted for extrapolating to environmentally relevant human exposures.[66] O_3 concentrations of 0.2 to 0.3 ppm are frequent in areas of high air pollution, similar to 1 ppm O_3 exposure in rodents.[41,69] Regarding single exposures, 2 ppm was used to compensate for rodent insensitivity, as previously reported.[42] Rochester-style Hinners chambers were used for whole-body O_3 inhalation exposure. The mice were placed in wire mesh individual housing cages that were transferred to the chambers for exposure. Before the experiment, mice were habituated to the exposure chambers for 5 consecutive days (4 hours/day).

RESEARCH IN CONTEXT

1. **Systematic review**: We reviewed articles in PubMed with combinations of keywords "astrocytes," "Alzheimer's disease," "air pollution," and "ozone." We found very little and limited work on the effects of urban air pollution on astrocytes, and how ozone (O_3) exposure affects astrocytic phenotype in Alzheimer's disease (AD) model is mostly unexplored.
2. **Interpretation**: Our findings indicate that O_3 exposure dysregulates astrocytes, where the specific proteomic and transcriptomic effect is dependent on localization near or away from plaques. We demonstrate that the disease-associated astrocyte (DAA) phenotype that is important in responding to amyloid plaques is perturbed by the O_3-induced lung–brain axis response and the consequent interacting communication between astrocytes and peripheral myeloid cells.
3. **Future directions**: Here, we highlight the important role of astrocytes in the lung–brain axis and the mechanisms by which the peripheral immune response to air pollution modulates this pathway, which is linked to augmented amyloid pathology. The detailed cellular mechanisms require significant additional inquiry. While we revealed O_3 dysregulation of the DAA phenotype associated with increased plaque load features increased cellular contact with microglia in the plaque microenvironment, the mechanistic underpinnings and impact on AD physiology require further exploration. Finally, this work also points to the vasculature as another point of impact in AD pathology that is of significant concern in understanding these complex mechanisms in future inquiry.

2.4 | Exposure-specific experimental design

For each study, animals were assigned to experimental groups using a randomized block design. Random numbers were generated using http://www.jerrydallal.com/random/randomize.htm.

2.4.1 | Subchronic O_3 exposure

For the subchronic O_3 exposure experiments exploring how astrocytes are modified during O_3-augmented amyloid plaque pathology, 120 male 10- to 11-week-old 5xFAD mice and littermate controls were exposed in two separate experiments (60 for CNS and 60 for pulmonary measures) to filtered air (FA), 0.3, or 1.0 ppm O_3 for 4 hours/day, 3 consecutive days/week, for 13 weeks ($n = 10$ per group). The mice were then euthanized, and samples were collected 18 tot 24 hours after the last exposure, as reported previously.[29] Because the

purpose of the study was to determine how O_3 modified the astrocyte phenotype during ongoing O_3-augmented amyloid pathology, the littermate control strain (no plaques) and the mice exposed to 0.3 ppm O_3 (no O_3-induced change in plaque pathology[29]) were excluded from processing and analysis.

2.4.2 | Single O_3 exposure

Two studies were conducted to investigate the effects of O_3 in *Hmgb1*$^{fl/fl}$.*LysM*-Cre^{+} mice. For the single 1.0 ppm exposure, 17 male 6- to 8-week-old *Hmgb1*$^{fl/fl}$. *LysM*-Cre^{+} mice and *Hmgb1*$^{fl/fl}$.*LysM*-Cre^{-} mice were exposed to 1.0 ppm O_3 or FA once for 4 hours (n = 4–5 mice). Samples were collected 18 to 24 hours after exposure. To obtain clear neuroimmune measurements in this unique strain and genetic background, the exposure was increased to a single 2.0 ppm O_3 exposure, which results in increased neuroimmune responses in the control *Hmgb1*$^{fl/fl}$.*LysM*-Cre^{-} mice.[29] As such, 38 male 6- to 8-week-old *Hmgb1*$^{fl/fl}$.*LysM*-Cre^{+} mice and *Hmgb1*$^{fl/fl}$. *LysM*-Cre^{-} mice were exposed to 2.0 ppm O_3 or FA once for 4 hours (n = 4–5 mice). Tissue samples were collected approximately 24 hours after exposure.

2.4.3 | rHMGB1 IV administration

Sixteen male C57Bl/6J mice (6–7 weeks old; n = 8) were injected intravenously by tail vein with 32.5 µg rHMGB1 (Thermo Scientific, 34-8401-85) in 200 µL vehicle (20 mM Tris HCl, pH 8.0, 0.2 M NaCl, 1 mM DTT). Three hours after injection, the mice were euthanized, and samples were collected. Samples were excluded from analysis when identified as statistical outliers, resulting in a final sample size of n = 6 to 8.

2.5 | Sample collection

2.5.1 | Brain tissue

Mice were euthanized with isoflurane. One brain hemisphere was microdissected (cortex, hippocampus, and midbrain), flash-frozen in liquid nitrogen, and stored at −80°C. The other half of the brain was fixed in 4% paraformaldehyde (Electron Microscopy Sciences, 1921) by immersion for 2 days, followed by cryopreservation in 30% sucrose in phosphate-buffered saline (PBS) for another 2 days. Then, the entire hemisphere was embedded with optimal cutting temperature compound (4583, Sakura Finetec) in cryomolds (Tissue-Tek, 4557, Sakura Finetec).

2.5.2 | Pulmonary samples

Bronchoalveolar lavage (BAL) fluid was collected from euthanized mice by lavaging the lung twice with 1 mL Hanks Balanced Saline Solution (21-622CV, Corning) without Ca^{2+} and Mg^{2+}. BAL fluid samples were centrifuged at 1500 × g for 10 minutes at 4°C, and the cell pellets were resuspended in 250 µL of PBS. Total cell counts were determined using a TC-10 automated cell counter (Bio-Rad), applied to slides using a Shandon Cytospin centrifuge (Thermo Scientific), and stained with Wright–Giemsa (89013, Thermo Scientific). Cell differentials were determined at 40× by a blinded observer counting at least 300 cells per sample.

2.6 | Fluorescent immunohistochemistry

Sagittal sections (40 µM) were collected using a freezing stage microtome (Microm HM 450, Thermo Scientific). For all following immunohistochemistry (IHC) endpoints, three evenly spaced sections approximately 0.24 mm apart spanning the motor cortex starting at the sagittal plane ≈ 0.6 mm lateral to the midline[70] were stained per brain. All sections were washed for 10 minutes in 0.1% PBS with Tween 20 (PBST) prior to antigen retrieval. Antigen retrieval was performed in 1 M sodium citrate solution at 85°C for 15 minutes with subsequent cooling to room temperature for 20 minutes. Blocking was performed with normal donkey serum for 1 hour, followed by overnight incubation in primary antibody diluted (1: 500) in blocking serum. Rabbit anti-GFAP (Agilent DAKO, Z0334; RRID AB_10013382) and goat anti-ionized calcium-binding adapter molecule 1 (IBA1; Novus Biologicals, NB100-1028) were used to stain astrocytes and microglia, respectively. Sections were washed three times in 0.1% PBST and incubated with secondary Alexa Fluor antibodies diluted (1:1000) in blocking serum at room temperature for 1 hour, followed by three washes with 0.1% PBST. Donkey anti-rabbit 647 (Invitrogen A-31573; RRID AB_2536183) and donkey anti-goat 488 (Invitrogen A11055; RRID AB_2534102) were used as secondary antibodies for GFAP and IBA1 staining, respectively. Sections were mounted on slides with Prolong Gold (P36930, Life Technologies), cover slipped, and dried overnight in the dark. Slides were stored at −20°C before imaging. To stain for Aβ plaques, sections were washed in 0.1% PBST for 5 minutes and Methoxy x34 (SL 1954, Millipore Sigma) solution (0.04 g X34 in 400 mL 100% ETOH and 600 mL DI H_2O) for 10 minutes. The slides were then sequentially washed five times with DDH_2O and 0.1% PBST for 5 minutes before the addition of Prolong Gold and coverslipping.

2.7 | Imaging

2.7.1 | Whole-cortex GFAP expression

The entire hemisphere was scanned at 10× using a Leica Aperio Versa slide scanner (Leica Microsystems Inc.) to determine whole-cortex astrocyte expression. Images were processed and analyzed using ImageJ (FIJI, version 2.9.0, NIH). The region of interest (ROI) was drawn around the entire cortex and manually thresholded. The Analyze Particles plugin was used to quantify the GFAP-positive area and

cell number. A sample size of 8 to 10 mice per group was analyzed per endpoint. Statistical outliers were excluded.

2.7.2 | Plaque-associated astrocyte quantification

For plaque-associated astrocyte quantification, 1 µm Z-stacks were acquired at 40× with oil immersion with a Nikon A1R confocal microscope in the primary motor region of the cortex due to ease of identification of the finite region using confocal microscopy. Images were analyzed in NIS Elements AR (Nikon) using the General Analysis 3 module. Image stacks were thresholded using consistent criteria across the entire analysis. To consistently define the plaque microenvironment, a 50 µm diameter circle was drawn around a plaque-positive area of this specific size, defining the periplaque ROI. A blinded observer counted GFAP-positive cell bodies manually in the maximum intensity projection image. Astrocytes were considered periplaque astrocytes if either the cell body or any branches were contained in the ROI. A sample size of 8 to 10 mice per group was analyzed per endpoint. Statistical outliers were excluded.

2.7.3 | Colocalized astrocyte–microglia volume quantification: cell–cell contact

To assess astrocyte–microglia colocalization, 1 µm spaced Z-stacks were acquired from the primary motor region of the cortex at 40× with oil immersion with a Nikon A1R confocal microscope. Images were analyzed in NIS Elements AR using the General Analysis 3 Module. Image stacks were thresholded using criteria maintained across the entire analysis. Within a 50 µm diameter ROI, areas double positive for GFAP and IBA1 were quantified per stack. The total colocalized volume was obtained by adding the colocalized area of all the stacks in the image and normalized by the total GFAP volume. A sample size of 8 to 10 mice per group was analyzed per endpoint. Statistical outliers were excluded.

2.8 | NanoString GeoMx digital spatial profiling: protein expression

Fixed 10 µm coronal sections were acquired with a cryostat (CM1900, Leica) and stored at −20°C before processing. Slides were processed per the NanoString Slide Prep manual for protein analysis. Briefly, slices were incubated with the NanoString GeoMx Alzheimer's Morphology kit, which contains the Aβ antibody for plaque visualization and Alexa Fluor 647-conjugated mouse anti-GFAP antibody (BioLegend, 837512; RRID AB_2734611) for astrocyte identification, along with NanoString panels (Neural Cell Profiling Core, Alzheimer's Disease Panel, Alzheimer's Disease Extended Panel, Glial Subtyping Panel) containing ≈ 60 antibodies with unique photo-cleavable oligonucleotide tags. Slices were scanned in the NanoString Digital Spatial Profiler, and polygonal ROIs were drawn around plaque-associated and non–plaque-associated astrocytes in the cortex. The GFAP-positive area within each ROI was delineated for photocleavable oligonucleotides collection. The collected oligonucleotides were hybridized with NanoString codeset, per the NanoString user manual, to map the counts to corresponding antibodies and region from where the oligonucleotides were collected. Digital counts were generated on an nCounter Max/Flex system (NanoString Technologies). The differential protein expression analysis was performed using the NanoString GeoMx Digital Spatial Profiling (DSP) Analysis Suite. The digital counts were tested for quality control and normalized to the housekeeping protein (GAPDH and histone H3) counts. Three sections were scanned per brain from a sample size of four animals per exposure group (FA or 1.0 ppm O_3) for the analysis, resulting in 68 to 70 ROIs analyzed per experimental group. ROIs that did not pass the quality control checks were excluded.

2.9 | NanoString GeoMx digital spatial profiling: whole transcriptome assay

Fixed frozen 10 µm coronal brain sections were processed with the NanoString Mouse Whole Transcriptome Atlas (WTA) panel per the NanoString user manual for spatial transcriptomic analysis. Plaques and astrocytes were visualized using Alexa Fluor 594-conjugated mouse anti-Aβ antibody (BioLegend 803019; RRID AB_2734552) and Alexa Fluor 647-conjugated mouse anti-GFAP antibody (BioLegend; 837512 RRID AB_2734611), respectively. Sections were scanned in the NanoString Digital Spatial profiler, and polygonal ROIs were drawn around plaque-associated astrocytes in the cortex. Photocleavable oligonucleotides were collected only from the GFAP-positive segments. Collected oligonucleotides were sequenced using the Illumina Next Generation Sequencing Platform (NanoString Technologies). Differential gene expression and enriched pathway analyses were conducted using the NanoString GeoMx DSP Analysis Suite. Normalization was performed using the ubiquitous astrocyte marker Aldh1l1[71,72] because its expression was unchanged in both groups. For the analysis, two to five sections were scanned per brain from a sample size of three animals per group, with 90 to 92 ROIs analyzed per experimental group. ROIs were excluded from the analysis if they did not pass the quality control test.

2.10 | RNA isolation and reverse transcription quantitative polymerase chain reaction

Microdissected whole cortex (including corpus collosum) and midbrain tissue were homogenized in Tissue Protein Extraction Reagent with protease and phosphatase inhibitors. An equal volume of TRIzol was added to each homogenate, and RNA was extracted per the manufacturers' protocol. RNA was treated with DNAse for purification using an Ambion DNA-free kit (Invitrogen AM1906) and reverse-transcribed using a Maxima First Strand cDNA synthesis kit (Invitrogen, K1641). Reverse transcription quantitative polymerase chain

reaction (RT–qPCR) was performed with 1 μL cDNA and TaqMan probes and primers (Tables S2 and S3) on a QuantStudio 6 Flex RT–PCR system (Applied Biosystems). *Gapdh* was used as the housekeeping control for $2^{-\Delta\Delta CT}$ quantification. For a complete list of primers and probes used, see Tables S2 and S3.

2.11 | Statistical analysis

Experimenters were blinded to the experimental groups. The sample size was determined according to prior reports, and power analyses were calculated for 80% power. Data were analyzed in GraphPad Prism 8.0 (GraphPad Prism). Outliers were determined using the ROUT method with Q = 1% and removed from all analyses. Normal distribution was tested using the Shapiro–Wilk test. A Welch *t* test was performed for data that passed the normality test. A two-way analysis of variance with Bonferroni post hoc analysis was performed when applicable. A *t* test was used for GeoMx DSP protein profiling and a linear mixed model with Benjamini–Hochberg post hoc correction for the whole transcriptome assay. Data are expressed as the mean ± standard error of the mean. A P value < 0.05 was considered to indicate significance.

3 | RESULTS

3.1 | Ozone exposure increases GFAP astrocyte density in the cortex

The role of astrocytes in maintaining neuronal health and function has been extensively studied and described.[46,53] Astrocytes are a heterogeneous and highly complex population of cells with unique phenotypic responses depending on pathological conditions. Some common characteristics of reactive astrocytes have been identified, such as the overexpression of GFAP with enlarged morphology,[46,49,53] which is a characteristic of AD.[46,49] However, the instigating events responsible for astrogliosis in AD and how astroglia respond to air pollution are poorly understood. Here, cortical GFAP-positive astrocytes were found to increase in number in response to O_3 exposure, as evidenced by increased O_3-elevated GFAP-positive cell counts and increased total cortical GFAP expression in 5xFAD mice (Figure 1A and B). To explore whether the O_3-induced increase in cortical astrocyte density is affected by plaque proximity, we quantified the plaque-associated and plaque-distant astrocyte numbers in confocal images of the primary motor cortex. Consistent with prior reports,[29] subchronic O_3 exposure increased the plaque number (Figure 1C and D). O_3 also increased the periplaque astrocyte number; however, only a trend toward an O_3-induced increase was observed in the number of non-plaque astrocytes (Figure S1A and S1B in supporting information). No significant difference in the number of periplaque astrocytes per plaque was identified (Figure 1E), suggesting that the close proximity of astrocytes to the higher number of plaques may be associated with the higher number of astrocytes. This association is further supported by the significant correlation between periplaque astrocytes and plaque number irrespective of O_3 exposure (Figure 1F). However, the number of non–plaque-associated astrocytes increased with O_3 exposure with no significant association with plaque number (Figure 1G), suggesting that O_3 affects astrogliosis differently depending on plaque localization.

3.2 | Ozone alters astrocyte-associated protein expression in the periplaque space

To understand how O_3 exposure and plaque localization could interact to affect the astrocyte phenotype and obtain insight into potential functional changes, we next sought to spatially profile cortical astrocyte protein expression according to their proximity to or distance from amyloid plaques. As such, we compared the protein expression pattern in periplaque astrocytes to that in astrocytes distant from the plaque deposition site (non-plaque) in both O_3- and FA-exposed mice. More specifically, we sought to elucidate how the astrocyte protein response to plaque deposition changes with O_3 exposure. DSP analysis revealed a baseline change in 25 astrocyte-associated proteins (Table S7 in supporting information) in periplaque astroctyes, consistent with prior findings.[49,53] Notably, the expression of 16 proteins changed regardless of O_3 exposure (Figure 2B). However, comparing plaque-associated and plaque-distant astrocytes, nine proteins (Figure 2B and C) were changed in only FA-exposed mice, including neprilysin and Ki-67, indicating a unique baseline change in plaque-associated astrocyte proteins that occurs without O_3 exposure. Thus, O_3 exposure appears to impede this shift in protein expression. However, myelin basic protein (MBP), CSF1R, and Clec7a protein expression levels were increased in response to O_3 in plaque-associated astrocytes (Table S7). The upregulation of microglia-associated proteins in response to O_3 in GFAP-positive tissue indicated increased cell-to-cell physical overlap, suggesting that O_3 may modify astrocyte–microglia communication in the plaque microenvironment.

3.3 | Ozone increases astrocyte and microglia colocalization in the plaque microenvironment

The overlapping GFAP-positive and IBA1-positive volume in the motor cortex periplaque space was calculated to directly test whether O_3 exposure affects astrocyte–microglia cell–cell contact around plaques (Figure 3A and Figure S2A in supporting information). The data demonstrated that O_3 exposure increased astrocyte and microglia colocalization in the plaque microenvironment (Figure 3B) but not in non-plaque regions (Figure 3C and D), suggesting that O_3 modifies glial cell–cell communication only near amyloid plaques. We have previously seen an O_3-induced decrease in plaque associated microglia,[29] making this increased colocalization even more intriguing. To verify that this increased colocalization is not simply a result of increased GFAP in the periplaque space, we normalized the data to total GFAP (Figure 3B). The significant difference was retained regardless of the source of GFAP volume.

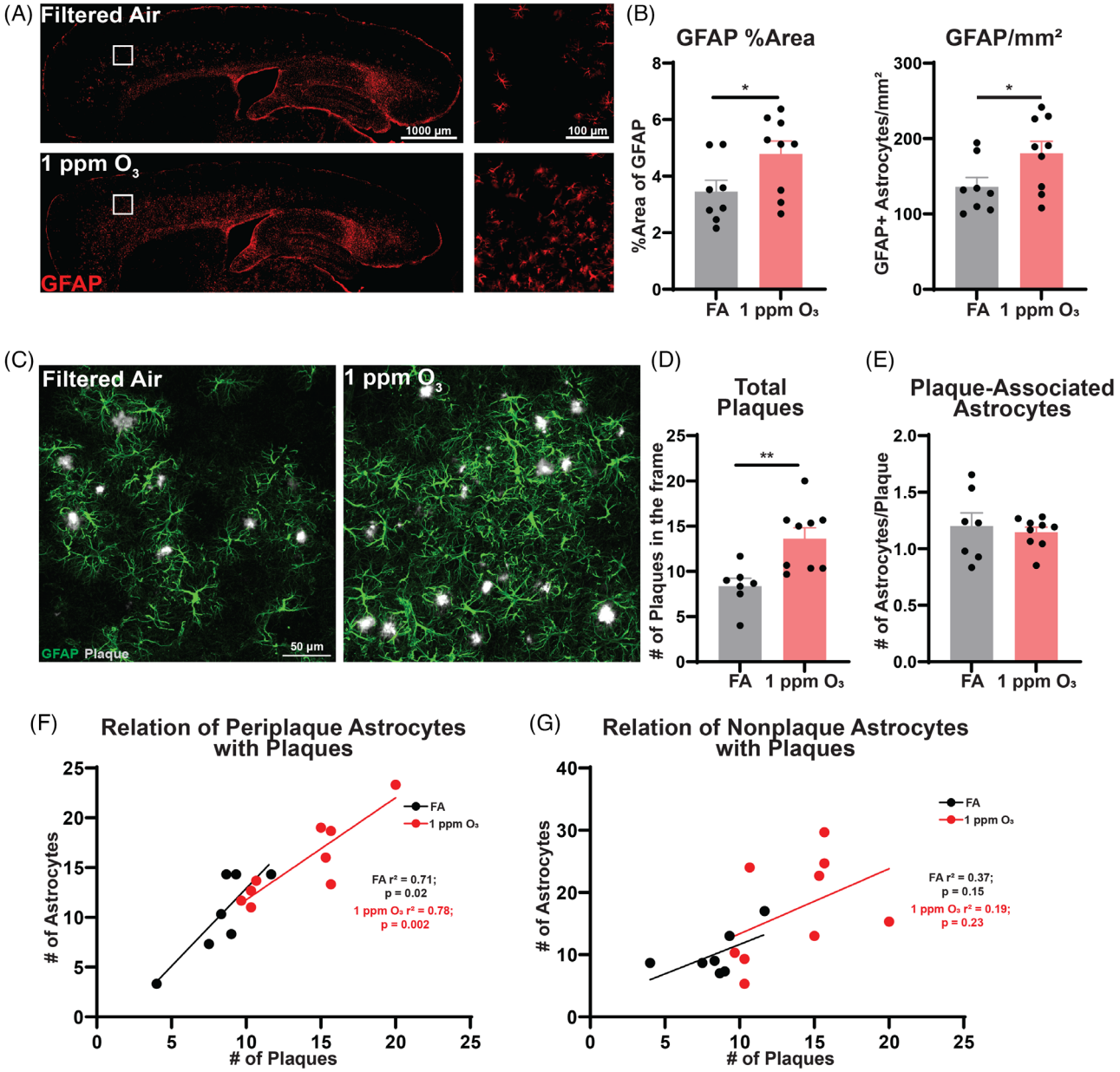

FIGURE 1 O_3 exposure increases astrocyte density in the cortex of 5xFAD mice. Male 5xFAD mice (10–11 weeks old) were exposed to either FA or 1.0 ppm O_3 for 3 consecutive days each week for 4 hours/day for 13 weeks. A, Representative 10× images depicting cortical astrocyte density (GFAP, red) in FA- and O_3-exposed mice. Scale bar: 1000 or 100 µm. B, Quantification of the number of GFAP-positive areas and GFAP-positive cells in the entire cortex (layers I–VI). C, Representative maximum intensity projection images taken at 40× in the cortex, staining for plaques (Methoxy-X34, gray) and astrocytes (GFAP, green). Scale bar: 50 µm. D, Quantification of plaque number in the 40× confocal images. E, Quantification of plaque-associated astrocytes normalized to plaque number. Correlation of the number of plaques with the number of (F) periplaque and (G) non-plaque astrocytes in the cortex. Astrocytes were considered periplaque if their cell bodies or branches reached within the circular periplaque region of interest drawn at 50 µm diameter around the plaque center; if not, they were considered nonplaque. Data are represented as the mean ± SEM, $n = 8–9$ mice/exposure group. * = $P < 0.05$; Welch t test. FA, filtered air; GFAP, glial fibrillary acidic protein; O_3, ozone; SEM, standard error of the mean

3.4 | Ozone triggers an astrocytic transcriptional shift

Large-scale astrogliosis is observed in AD, and impaired clearance of Aβ by astrocytes is thought to be deleterious.[49] A recently identified DAA population displays a somewhat distinct transcriptional phenotype when localized around plaques; however, this transcriptomic fingerprint is also closely linked with astrocyte subpopulations in the aged brain.[53] Very little is known about how air pollution exposure changes astrocytes, particularly the transcriptional phenotype of plaque-associated astrocytes. Thus, we used DSP and the NanoString WTA to assess the transcriptional changes in periplaque versus

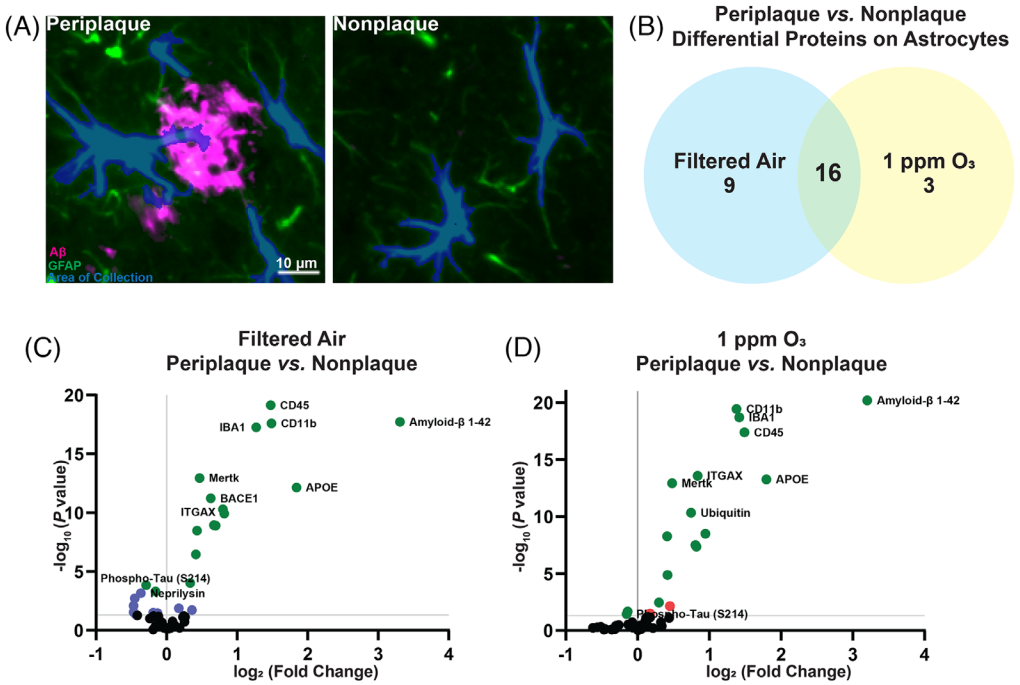

FIGURE 2 O_3 altered the astrocytic protein expression pattern, dependent on spatial localization with plaques. Male 5xFAD mice (10–11 weeks old) were exposed to FA or 1.0 ppm O_3 for 3 consecutive days each week for 4 hours/day for 13 weeks. A, Representative images from the NanoString GeoMX DSP platform illustrating periplaque (left) and non-plaque astrocytes (right), as defined by plaque staining (Aβ, magenta), astrocyte (GFAP, green) staining, and the area from which samples were collected for analysis (blue). Scale bar: 10 µm. B, Venn diagram showing the number of plaque environment-induced changes in the astrocyte proteomic profile in FA and O_3 groups, indicating protein changes shared between the two groups. Volcano plots representing differentially expressed proteins on periplaque versus plaque-distant astrocytes in the (C) FA and (D) O_3 groups. $n = 68–72$ ROIs/region per exposure group ($n = 4$ mice/exposure group). $P < 0.05$. Aβ, amyloid beta; DSP, Digital Spatial Profiling; FA, filtered air; GFAP, glial fibrillary acidic protein; O_3, ozone; ROI, region of interest

plaque-distant astrocytes in FA- and O_3-exposed 5xFAD mice. O_3 exposure triggered a unique transcriptional shift in periplaque astrocytes (Figure 4A and B). On closer examination of the differentially expressed genes in these astrocytes (Table S8 in supporting information), an accelerated DAA phenotype was present, highlighted by increased expression of serpina3n, a serine protease inhibitor associated with increased amyloid accumulation;[53,73] ctsb and ctsd, lysosomal cysteine proteases associated with amyloid precursor protein processing;[53,74] and *c1qa*, a complement factor associated with astrocyte-mediated synapse elimination.[75] However of the protein targets upregulated in the O_3 group, only csf1r, cd9, and ctsd were also significantly transcriptionally upregulated with DSP analysis. Pathway analysis revealed that O_3 upregulated several functional categories of genes in periplaque versus plaque-distant astrocytes, including cell–cell communication and gap junction trafficking pathways (Figure 4C and Table S9 and S10 in supporting information). O_3 also resulted in the downregulation of genes in other categories in periplaque but not plaque-distant astrocytes, such as matrix metalloproteinase (Figure 4D), suggesting extracellular matrix modifications potentially underlie the spatially defined differences. Overall, these results suggest O_3 triggers a potentially pathologically dysregulated astrocyte phenotype that occurs concomitantly with higher Aβ accumulation.

3.5 | Peripheral HMGB1 mediates O_3-induced dysregulation of astrocytes

We previously demonstrated that peripheral HMGB1 regulates the microglial response to O_3 in 5xFAD mice;[29] however, the impact on astrocytes is unknown. Here, HMGB1 mRNA levels were found to be downregulated in O_3-exposed BAL fluid (Figure 5A), predominantly comprising infiltrating myeloid cells consistent with prior studies in other tissues.[29,76] Thus, we hypothesized that peripheral myeloid cell HMGB1 is involved in the association between astrocytes and amyloid pathology. To test this hypothesis, we used the previously described *Hmgb1fl/fl.LysM*-Cre$^+$ mouse strain,[29] with HMGB1 specifically deleted in only peripheral myeloid cells, including BAL fluid cells. A single 4 hour O_3 exposure (1 ppm) reduced neutrophil and lymphocyte infiltration into the BAL fluid in *Hmgb1fl/fl.LysM*-Cre$^+$ mice (Figure 5B), indicating that myeloid cell HMGB1 plays an important role in peripheral immune cell trafficking and the pulmonary immune response to O_3. Given the reduced HMGB1 mRNA in these cells in 5xFAD mice after a 13 week exposure, we hypothesize that ongoing AD pathology and extended exposure length could have a differential impact on HMGB1 mRNA expression in these cells. Interestingly, serpina3n levels in the midbrain of *Hmgb1fl/fl.LysM*-Cre$^+$ mice were reduced in response to O_3 exposure (Figure 5C), further suggesting that peripheral myeloid

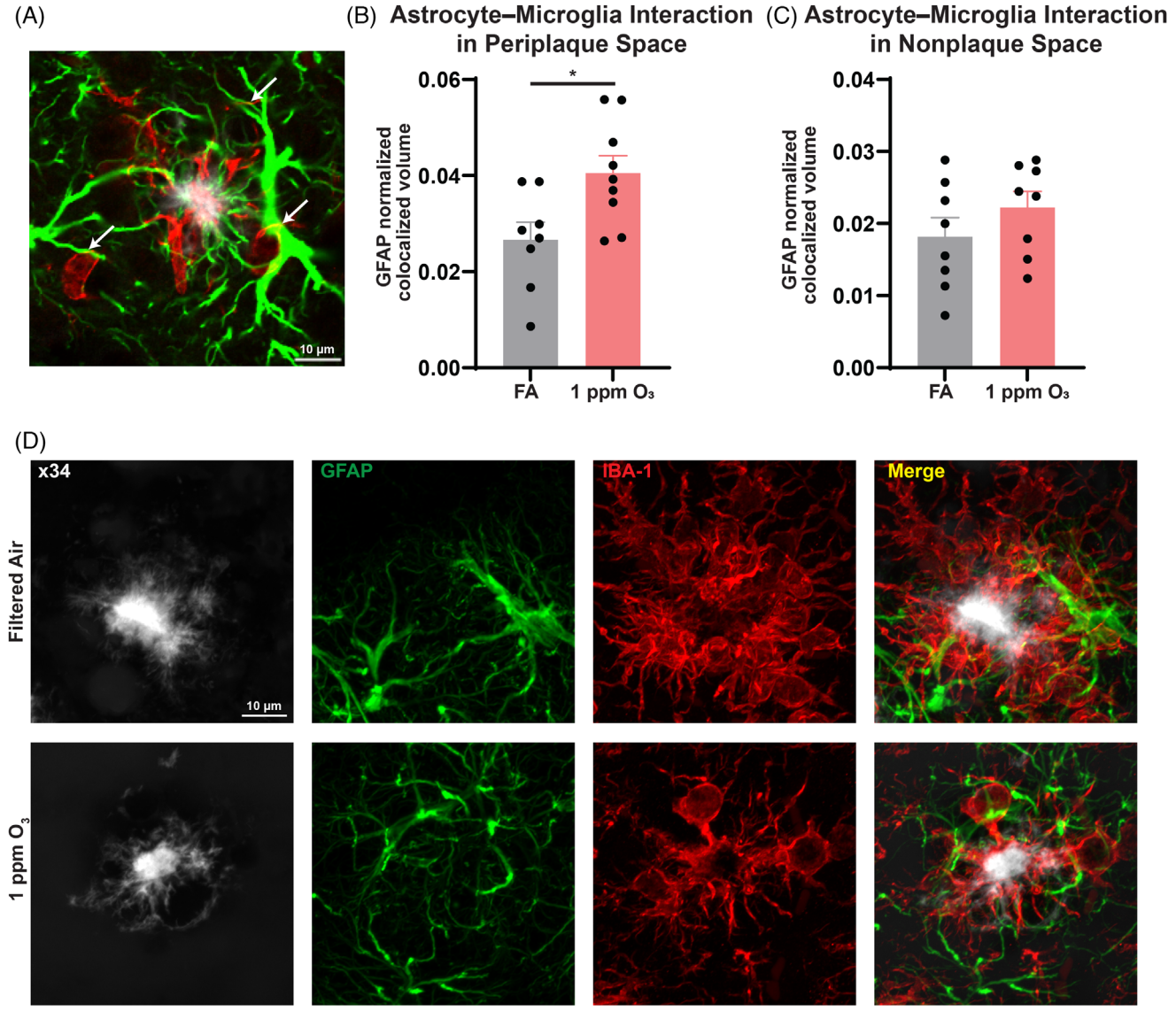

FIGURE 3 O_3 increased astrocyte–microglia cell contact in the plaque microenvironment. Male 5xFAD mice (10–11 weeks old) were exposed to either FA or 1.0 ppm O_3 for 3 consecutive days each week for 4 hours/day for 13 weeks. A,= Representative image showing colocalized areas (yellow) of cell–cell contact, as indicated by white arrows in a single image from a set of confocal Z-stack images taken at 40×. Scale bar: 10 µm. Quantification of astrocyte–microglia colocalization in the (B) periplaque and (C) non-plaque (right) space from confocal Z-stacks taken at 40× in the cortex. Data are represented as the mean ± SEM, $n = 8–9$ mice/exposure group. * = $P < 0.05$; Welch *t* test. D, Representative maximum intensity images taken at 60× showing plaques (Methoxy-X34, gray), astrocytes (GFAP, green), and microglia (IBA1, red) in the O_3 and FA groups. Scale bar: 10 µm. FA, filtered air; GFAP, glial fibrillary acidic protein; IBA1, ionized calcium-binding adapter molecule 1; O_3, ozone; SEM, standard error of the mean

cells and HMGB1 influence the expression of astrocyte genes in the lung–brain axis.

Circulating HMGB1 has previously been shown to be upregulated in 5xFAD mice in response to O_3.[29] Thus, we treated C57 mice with 32.5 µg recombinant HMGB1 protein intravenously, as previously reported,[29,77] to determine whether circulating HMGB1 can regulate the DAA phenotype. Circulating HMGB1 increased *Gfap* mRNA expression in the midbrain, and there was a trend toward an increase in c3, and aqpn4 mRNA expression (Figure 5D). Most of these DAA markers were demonstrated above to be modified by O_3 in the cortex in 5xFAD mice (Table S8). Overall, these data suggest that the peripheral myeloid cell HMGB1 is modified by O_3 exposure and may play an important role in immune cell trafficking and modulating the astrocytic response to O_3 exposure.

4 | DISCUSSION

O_3 is a major component of urban air pollution and abundant at levels deleterious to human health across the United States and worldwide.[24]

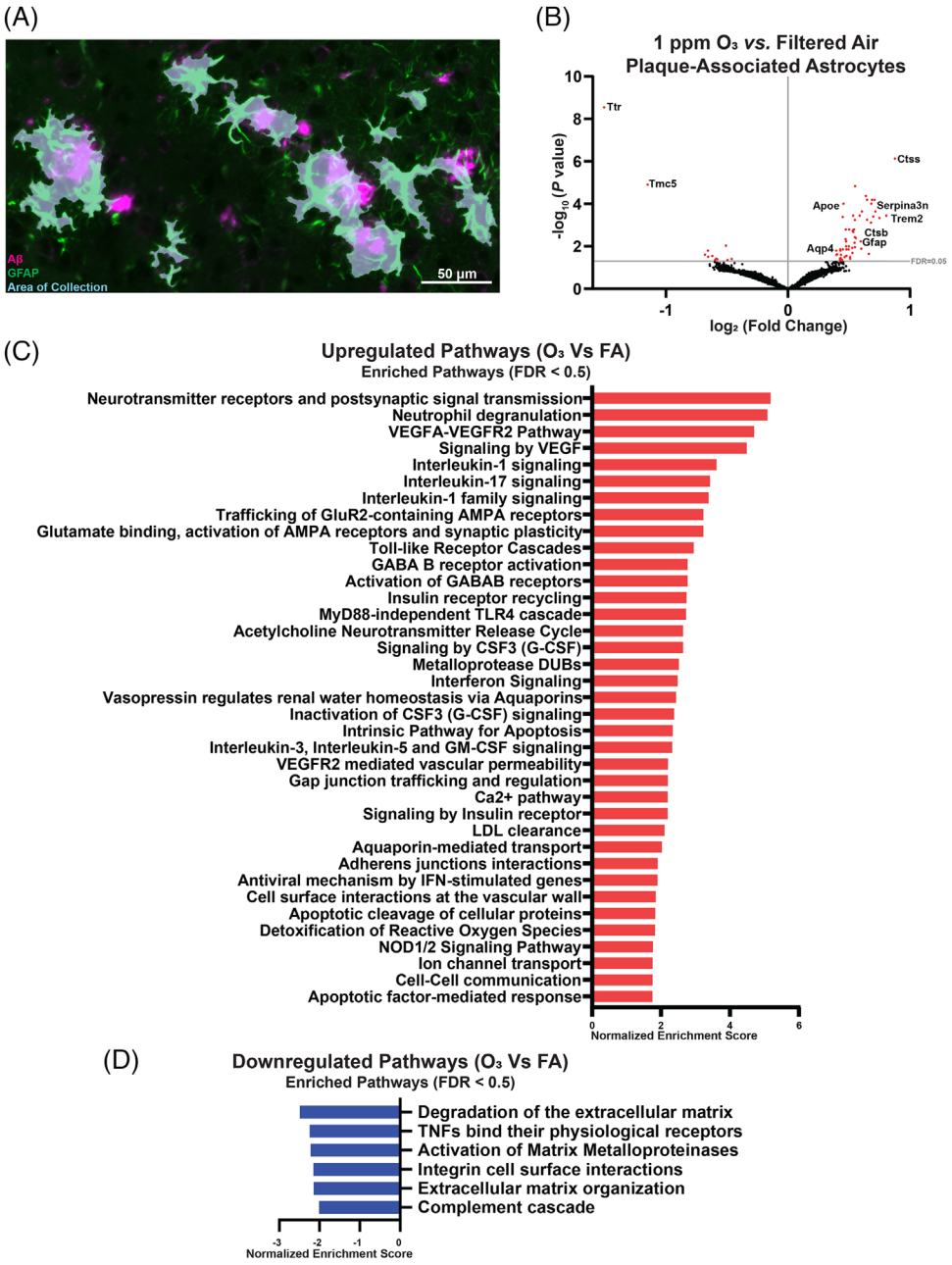

FIGURE 4 O_3 alters the astrocytic transcriptional profile in the plaque microenvironment. Male 5xFAD mice (10–11 weeks old) were exposed to either FA or 1.0 ppm O_3 for 3 consecutive days each week for 4 hours/day for 13 weeks. A, Representative image showing the digital spatial profiler scan for regions of interest containing astrocytes localized in the periplaque space, as defined by plaque staining (6e10, magenta), astrocyte staining (GFAP, green), and the area from which GFAP-positive cells were collected for mRNA analysis (blue). Scale bar, 50 µm. B, Volcano plot showing O_3-induced gene expression in plaque-associated astrocytes compared to that in the FA group. Highlighted genes represent a subset of significantly changed genes (red dots) after FDR correction (Benjamini–Hochberg, $P < 0.05$). Pathway analysis of O_3 versus FA cortical astrocyte gene expression in plaque-associated astrocytes depicting significantly (C) increased and (D) decreased pathways of interest (Benjamini–Hochberg, $P < 0.05$. $n = 96$ ROIs/region per exposure group ($n = 3$ mice/exposure group). FA, filtered air; FDR, false discovery rate; GFAP, glial fibrillary acidic protein; O_3, ozone; ROI, region of interest

High O_3 levels have recently been strongly associated with increased AD risk.[27] In addition, O_3 is associated with chronic obstructive pulmonary disease (COPD) and is a well-known asthma irritant,[78,79] and recent studies have linked both asthma[80] and COPD[81] to increased dementia risk, further emphasizing the importance of understanding the underlying disease mechanisms. In the current study, using 5xFAD mice, we explored the mechanistic underpinnings of how an inhaled gas incapable of translocating to the brain (O_3) could impact the brain and cellular pathology in the CNS parenchyma in association with peripheral immune responses. We define periplaque DAAs and

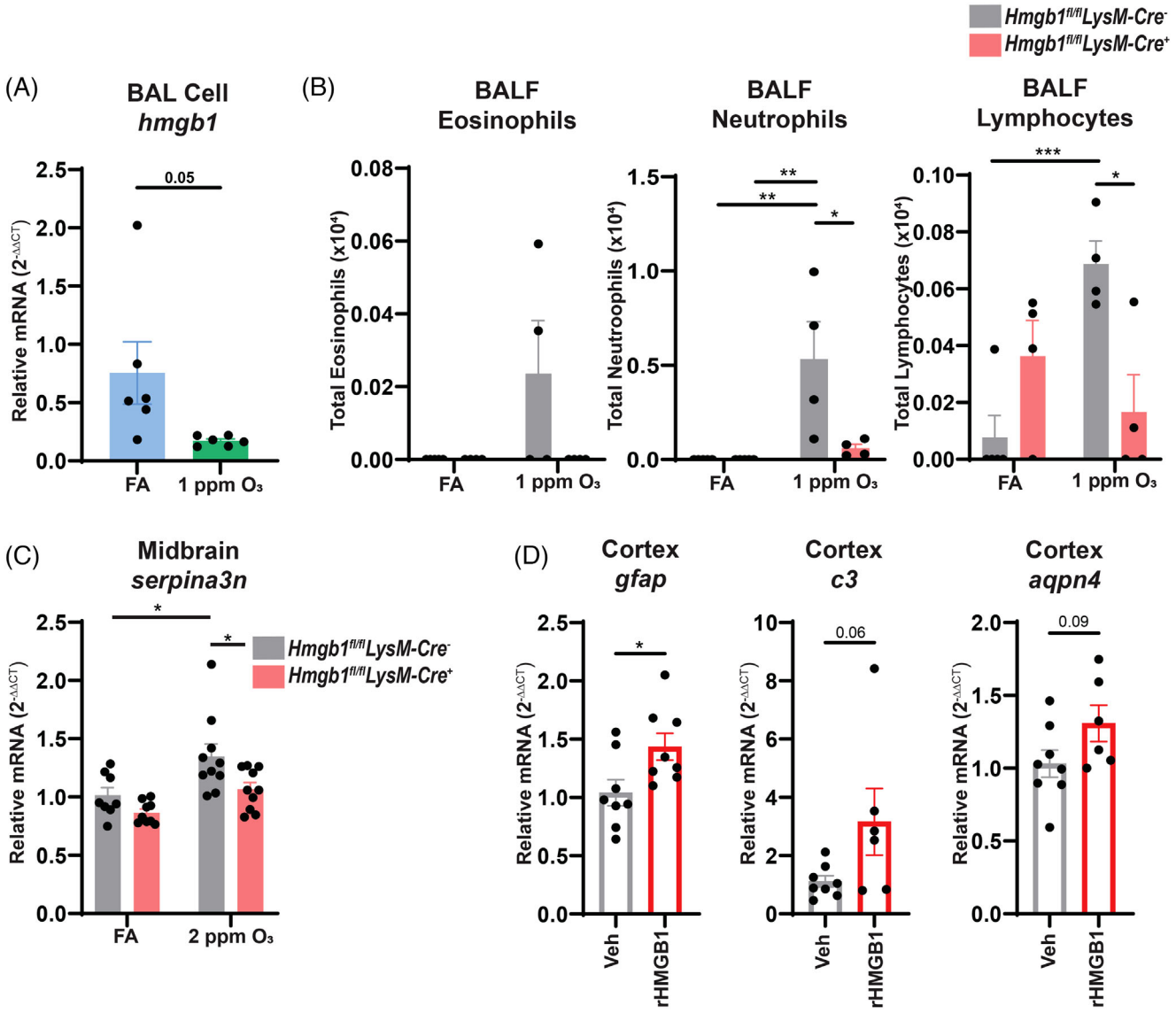

FIGURE 5 Peripheral HMGB1 modulates O_3-induced astrocytic dysregulation. A, Subchronic (13-week) O_3 (1 ppm) exposure reduced HMGB1 mRNA expression in the BAL cells of 5xFAD mice. Data are represented as the mean ± SEM, $n = 6$ mice/exposure group. Welch *t* test. B, *Hmgb1*$^{fl/fl}$*.LysM*-Cre^{+} mice have *Hmgb1* genetically ablated in peripheral myeloid cells (comprising a substantial component of BAL fluid cells) but not microglia. *Hmgb1*$^{fl/fl}$*.LysM*-Cre^{-} and *Hmgb1*$^{fl/fl}$*.LysM*-Cre^{+} mice were exposed to O_3 (1.0 ppm) or FA once for 4 hours. Cell counts of eosinophils, neutrophils, and lymphocytes infiltrating the BAL are shown. Data are represented as the mean ± SEM, $n = 3$–5 mice/group. * = $P < 0.05$, ** = $P < 0.01$, *** = $P < 0.001$; Welch *t* test. C, *Hmgb1*$^{fl/fl}$*.LysM*-Cre^{-} and *Hmgb1*$^{fl/fl}$*.LysM*-Cre^{+} mice were exposed to O_3 (2.0 ppm) or FA once for 4 hours. *Serpina3n* mRNA levels in the midbrain after a single 2 ppm O_3 exposure are shown. Data are represented as the mean ± SEM, $n = 9$–10 mice/exposure group. * = $P < 0.05$, †† = $P < 0.01$. D, *Gfap, C3, and Aqpn4* mRNA levels were assessed 3 hours after a tail vein injection of rHMGB1 (32.5 μg). Data are represented as the mean ± SEM, $n = 6$–8 mice/exposure group. * = $P < 0.05$; Welch *t* test. BAL, bronchoalveolar lavage; FA, filtered air; HMGB1, high mobility group box 1; O_3, ozone; SEM, standard error of the mean

demonstrate the involvement of peripheral myeloid cells in their regulation to delineate an overlooked component of the lung–brain axis that potentially influences how urban air pollution promotes AD pathobiology (Figure 6).

In the current study, we demonstrated that GFAP astrocyte density in the cortex of 5xFAD mice increases in response to O_3 exposure (Figure 1A and B). The number of plaque-associated astrocytes increased with O_3 exposure; however, the number of astrocytes surrounding each plaque did not increase. Thus, the increase in cortical astrocytes was likely due to the increase in the number of plaques in response to O_3 exposure (Figure 1E). Importantly, the astrocytes surrounding plaques, which are important for plaque clearance and reducing toxicity,[54,55] were found to be qualitatively different after O_3 exposure (Figures 2–4). Periplaque astrocytes from 5xFAD mice exposed to O_3 exhibited a localization-dependent altered astrocytic proteomic profile (Figure 2). On closer examination, many of the

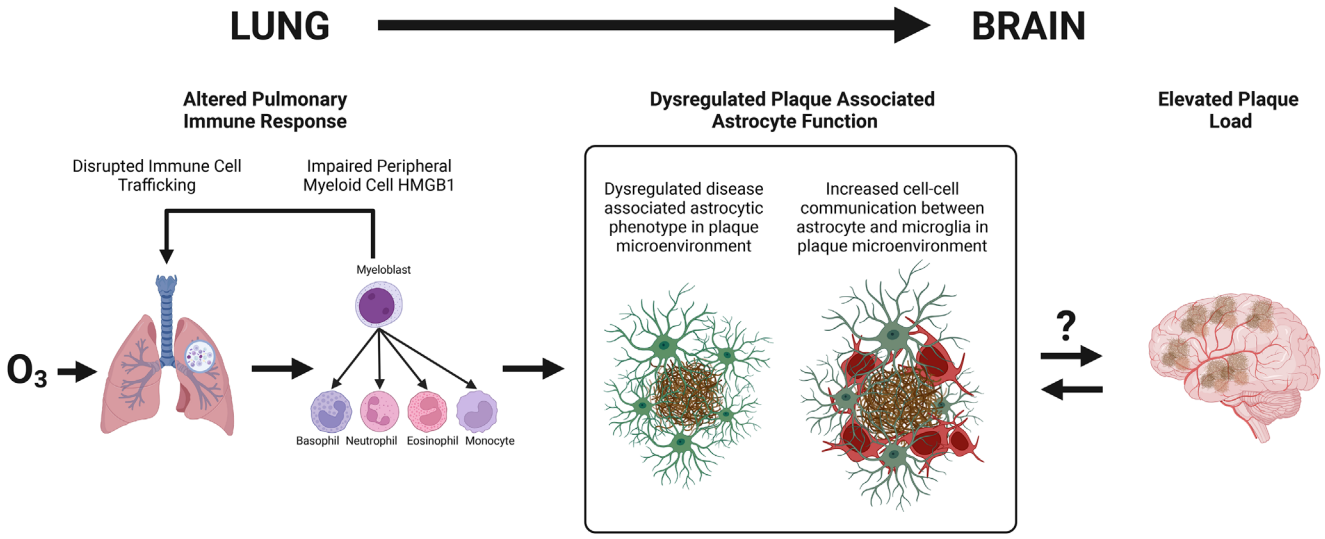

FIGURE 6 Plaque-associated astrocytes and peripheral myeloid cells interact in the O_3-dysregulated lung–brain axis: Implications for Alzheimer's disease. O_3, a reactive gas component of urban air pollution that cannot reach the brain, increased astrocyte density in the 5xFAD mouse cortex, concomitant with decreased bronchoalveolar lavage fluid cell (predominantly myeloid) HMGB1 expression and an exacerbated plaque burden. O_3-induced astrocyte effects (transcriptomic and proteomic) were dependent on the localization of astrocytes relative to plaques, indicating that this air pollution exposure selectively and qualitatively changes astrocytes in the plaque microenvironment, accelerates the astrocyte transcriptomic shift to a disease-associated astrocyte phenotype, and increases astrocyte contact with microglia but not plaques. Mechanistically, O_3-exposed mice with HMGB1 deleted from the peripheral myeloid cells but not microglia exhibited a perturbed pulmonary immune response to O_3 and disrupted DAA markers in the brain, indicating that peripheral myeloid cells and HMGB1 regulate the astrocyte DAA response to O_3. These findings provide much-needed insight into how urban air pollution may dysregulate the lung–brain axis, disrupt astrocytic function, and increase the amyloid burden. DAA, disease-associated astrocytes; HMGB1, high mobility group box 1; O_3, ozone

proteomic changes occurring only with O_3 exposure in plaque-distant versus periplaque astrocytes involved the loss of several key proteins (Figure 2). Some unexpected proteins, such as MBP, were upregulated in plaque-associated astrocytes in response to O_3 exposure (Table S7). This finding suggests that astrocytes may take up MBP during neurite breakdown, consistent with our prior work showing that O_3 enhances dystrophic neurites in the periplaque space.[29]

Importantly, the upregulation of microglia-specific proteins in astrocytes (Table S7) likely reflects an increase in cell–cell interactions and communication between astrocytes and microglia in the plaque microenvironment. We directly tested increased astrocyte–microglia interactions by IHC (Figure 3) and demonstrated that O_3 increases astrocyte–microglia contact only in the periplaque space. Additionally, these periplaque cells differ transcriptionally from plaque-distant astrocytes, demonstrating altered cell–cell communication and gap junction trafficking pathway genes in the plaque microenvironment (Figure 4). It has been previously reported that microglia and astrocyte cell–cell contact may be important for amyloid clearance.[82] We hypothesize that increased astrocyte–microglia communication may signify a coordinated effort between these cell types in compensating for the O_3 exposure–induced dysregulation of protective functions in the periplaque space.

While O_3 mainly induced a loss of protein expression in periplaque astrocytes, a larger transcriptional inquiry revealed the upregulation of genes such as *serpina3n*, *c1qa*, *c1qb*, and *ctsb*, indicating that O_3 exposure shifted the astrocyte transcriptional signature toward a more enriched DAA phenotype. Among the DAA genes upregulated by O_3 only in the periplaque space, *serpina3n* is associated with increased Aβ deposition and could contribute to increased plaque burden.[53,73] Notably, DAA astrocytes precede plaque deposition in 5xFAD mice and accumulate over time.[53] Here, exposure to O_3 appears to accelerate the DAA phenotype in 5xFAD mice. However, while this O_3-accelerated DAA phenotype correlated with an O_3-induced increase in plaque burden in the current study, the beneficial or deleterious consequences of the O_3-modified astrocyte genes in the periplaque space remain unclear and require substantial further investigation.

The transcriptional data emphasize that O_3 exposure qualitatively changes periplaque astrocytes, revealing multiple important potential targets for future mechanistic inquiry. For example, O_3 exposure has a well-established impact on stroke and vascular pathology,[30,37,83] and the astrocyte gene expression pathway analysis in the current study denotes changes in pathways involving vascular wall communication, vegfa–vegr2 communication (which occurs in vascular endothelial cells), and aquaporin communication, all of which point to O_3-induced phenotypic changes in plaque-associated astrocytes that may be linked to neurovascular dysfunction or pathology. Interestingly, gene expression changes in neurotransmitter pathways were also altered, which is unsurprising because astrocytes are known to maintain neurotransmitter homeostasis, the disruption of which is neurotoxic. This finding supports our previous data showing that O_3 exposure augments neuritic dystrophy.[29]

We next sought to better understand the mechanisms underlying these changes in the periplaque astrocyte phenotype. Peripheral immune cells traffic to the lung upon O_3 inhalation,[84] and these cells and their associated circulating factors are key components of the lung–brain axis.[41] Here, we discovered that with subchronic O_3 exposure in 5xFAD mice, when the plaque load was increased and the proteomic and transcriptomic DAA phenotype was disrupted, HMGB1 gene expression was lowered in the immune (predominantly myeloid) cells that trafficked to the lung (Figure 5). While this decrease in gene expression does not demonstrate a direct impact on Aβ plaque load it implies a potential relation to be directly tested in future studies. Furthermore, peripheral myeloid cell-specific HMGB1 deletion reduced immune cell infiltration into the lung and midbrain *serpina3n* expression (Figure 5), implicating the lung–brain axis in modulating the astrocytic transition to the DAA phenotype. Our data demonstrating that circulating HMGB1 upregulates DAA marker expression further indicate that peripheral HMGB1 influences the periplaque astrocyte phenotype.

Overall, our findings demonstrate that O_3 triggers a qualitative change in periplaque astrocytes, dysregulates cell–cell communication and cellular function in the plaque microenvironment, and accelerates the astrocyte transcriptomic shift toward the DAA phenotype, which is associated with an increased plaque number. These findings identify astrocytes, particularly periplaque astrocytes, as a key mechanistic component of the lung–brain axis associated with the effect of air pollution on AD pathology. Finally, we demonstrate the important role of peripheral HMGB1 in this process, highlighting a critical need to investigate this highly complex mechanistic pathway further.

One limitation of this study is the use of the 5xFAD mouse model. While this model is popular for investigating amyloid pathology, the AD phenotype is aggressive, particularly in female mice. This prevented us from assessing female mice in this study, and sex-based differences may exist. Additionally, the focus of this study was astrocytic dysregulation in the context of amyloid pathology. To fully elucidate the role of the lung–brain axis in astrocytic dysregulation in AD, its effects on tau pathology must be investigated in the future.

While O_3 is unable to directly interact with the brain parenchyma after inhalation, it is important to note that in addition to the pulmonary epithelium, O_3 also reacts with nasal epithelium potentially causing some lesions and generating cytokines among other factors that could also be an indirect pathway signaling O_3-induced CNS effects, which is a point of future study, to fully elucidate how O_3 affects the brain.

This article introduces a complex mechanism implicating astrocytes in the lung–brain axis that will require extensive multidisciplinary studies to fully elucidate. The following prospects for future inquiry were identified according to our results: (1) The identification and localization of the culpable immune cell cascade, tracing the first immune cell response in the periphery to the transfer of the cascade to the brain parenchyma and subsequent follow-up of chronic consequences. (2) An exploration of the CNS cellular contribution and the role of cell–cell contact, including the CNS vasculature unit and border-associated macrophages, in how O_3 communicates with the brain and impacts astrocyte and amyloid pathology. (3) Rescue studies investigating whether peripheral circulating factors can ameliorate the O_3-augmented astrocyte and amyloid pathology. (4) Investigations into the O_3 lung–brain axis exposome and its role in this process, comparing identifiable markers of pathological peripheral immune changes, deleterious circulating factors, ongoing astrocyte disruption, and amyloid pathology in AD animal models exposed to O_3 with those in AD, asthma, and COPD patient data.

This study is the first to identify astrocytes as part of the lung–brain axis and explore how trafficking immune cells can modify astrocytes and, potentially, amyloid plaque pathology in response to air pollution. Together, these findings provide much-needed insight into the underlying mechanisms driving how exposure to high levels of air pollutants, such as O_3, increases AD risk, highlighting the need to investigate this complex mechanistic pathway further to deepen our understanding of AD etiology, identify targets for the prevention and treatment of this disease, and guide the development of policies regulating air pollution.

ACKNOWLEDGMENTS

We thank the Stark Neurosciences Research Institute Biomarker core for guidance and assistance with NanoString GeoMx DSP studies and the Center for Medical Genomics core for sequencing oligonucleotides collected from NanoString GeoMx WTA. We are grateful to the IU School of Medicine Large Animal Resource Center, particularly Katie Culver, for their continued support with our mice. This study was graciously funded and supported by NIH 1RF1AG077826 and supported by the VA Merit Award I01 BX004161, NIH RO1 ES029835GW, and NIH R01 ES028104 awarded to Michelle L. Block.

CONFLICT OF INTEREST STATEMENT

The authors have no competing interests to declare. Author disclosures are available in the supporting information.

CONSENT STATEMENT

No human subjects were used in this study and consent was not required.

ORCID

Michelle L. Block https://orcid.org/0000-0001-8303-7914

REFERENCES

1. Knopman DS, Amieva H, Petersen RC, et al. Alzheimer disease. *Nat Rev Dis Primers*. 2021;7:33. doi:10.1038/s41572-021-00269-y
2. Masters CL, Bateman R, Blennow K, Rowe CC, Sperling RA, Cummings JL. Alzheimer's disease. *Nat Rev Dis Primers*. 2015;1:15056. doi:10.1038/nrdp.2015.56
3. Adani G, Filippini T, Garuti C, et al. Environmental risk factors for early-onset Alzheimer's dementia and frontotemporal dementia: a case-control study in northern Italy. *Int J Environ Res Public Health*. 2020;17:7941. doi:10.3390/ijerph17217941
4. Knobel P, Litke R, Mobbs CV. Biological age and environmental risk factors for dementia and stroke: molecular mechanisms. *Front Aging Neurosci*. 2022;14:1042488. doi:10.3389/fnagi.2022.1042488
5. Haghani A, Cacciottolo M, Doty KR, et al. Mouse brain transcriptome responses to inhaled nanoparticulate matter differed by sex and APOE

in Nrf2-Nfkb interactions. *eLife*. 2020;9:e54822. doi:10.7554/eLife.54822
6. Armstrong TD, Suwannasual U, Kennedy CL, et al. Exposure to traffic-generated pollutants exacerbates the expression of factors associated with the pathophysiology of Alzheimer's disease in aged C57BL/6 wild-type mice. *J Alzheimers Dis*. 2020;78:1453-1471. doi:10.3233/JAD-200929
7. Richardson JR, Roy A, Shalat SL, et al. Elevated serum pesticide levels and risk for Alzheimer disease. *JAMA Neurol*. 2014;71:284. doi:10.1001/jamaneurol.2013.6030
8. Bolton JL, Marinero S, Hassanzadeh T, et al. Gestational exposure to air pollution alters cortical volume, microglial morphology, and microglia-neuron interactions in a sex-specific manner. *Front Synaptic Neurosci*. 2017;9:10. doi:10.3389/fnsyn.2017.00010
9. Gao Q, Zang E, Bi J, et al. Long-term ozone exposure and cognitive impairment among Chinese older adults: a cohort study. *Environ Int*. 2022;160:107072. doi:10.1016/j.envint.2021.107072
10. Calderón-Garcidueñas L, Leray E, Heydarpour P, Torres-Jardón R, Reis J. Air pollution, a rising environmental risk factor for cognition, neuroinflammation and neurodegeneration: the clinical impact on children and beyond. *Rev Neurol*. 2016;172:69-80. doi:10.1016/j.neurol.2015.10.008
11. Block ML, Calderón-Garcidueñas L. Air pollution: mechanisms of neuroinflammation and CNS disease. *Trends Neurosci*. 2009;32:506-516. doi:10.1016/j.tins.2009.05.009
12. Paul KC, Haan M, Mayeda ER, Ritz BR. Ambient air pollution, noise, and late-life cognitive decline and dementia risk. *Annu Rev Public Health*. 2019;40:203-220. doi:10.1146/annurev-publhealth-040218-044058
13. Iaccarino L, La Joie R, Lesman-Segev OH, et al. Association between ambient air pollution and amyloid positron emission tomography positivity in older adults with cognitive impairment. *JAMA Neurol*. 2021;78:197. doi:10.1001/jamaneurol.2020.3962
14. Semmens EO, Leary CS, Fitzpatrick AL, et al. Air pollution and dementia in older adults in the Ginkgo evaluation of memory study. *Alzheimers Dement*. 2023;19:549-559. doi:10.1002/alz.12654
15. Zare Sakhvidi MJ, Yang J, Lequy E, et al. Outdoor air pollution exposure and cognitive performance: findings from the enrolment phase of the CONSTANCES cohort. *Lancet Planet Health*. 2022;6:e219-e229. doi:10.1016/S2542-5196(22)00001-8
16. Shi L, Wu X, Danesh Yazdi M, et al. Long-term effects of PM2·5 on neurological disorders in the American Medicare population: a longitudinal cohort study. *Lancet Planet Health*. 2020;4:e557-e565. doi:10.1016/S2542-5196(20)30227-8
17. Bhatt DP, Puig KL, Gorr MW, Wold LE, Combs CK. A pilot study to assess effects of long-term inhalation of airborne particulate matter on early Alzheimer-like changes in the mouse brain. *PLoS One*. 2015;10:e0127102. doi:10.1371/journal.pone.0127102
18. Zhang JJ, Wei Y, Fang Z. Ozone pollution: a major health hazard worldwide. *Front Immunol*. 2019;10:2518. doi:10.3389/fimmu.2019.02518
19. *WHO Global Air Quality Guidelines*. WHO; 2021.
20. Air Quality—National Summary. n.d. https://www.epa.gov/air-trends/air-quality-national-summary
21. U.S. EPA. Integrated Science Assessment (ISA) for Ozone and Related Photochemical Oxidants (Final Report, *Feb 2013*). U.S. Environmental Protection Agency; 2013. EPA/600/R-10/076F. n.d.
22. Zhao N, Pinault L, Toyib O, Vanos J, Tjepkema M, Cakmak S. Long-term ozone exposure and mortality from neurological diseases in Canada. *Environ Int*. 2021;157:106817. doi:10.1016/j.envint.2021.106817
23. Murray CJL, Aravkin AY, Zheng P, et al. Global burden of 87 risk factors in 204 countries and territories, 1990-2019: a systematic analysis for the Global Burden of Disease Study 2019. *Lancet North Am Ed*. 2020;396:1223-1249. doi:10.1016/S0140-6736(20)30752-2
24. World Health Organization, eds. *Air Quality Guidelines: Global Update 2005: Particulate Matter, Ozone, Nitrogen Dioxide, and Sulfur Dioxide*. World Health Organization; 2006.
25. Chen J-C, Schwartz J. Neurobehavioral effects of ambient air pollution on cognitive performance in US adults. *Neurotoxicology*. 2009;30:231-239. doi:10.1016/j.neuro.2008.12.011
26. Cleary EG, Cifuentes M, Grinstein G, Brugge D, Shea TB. Association of low-level ozone with cognitive decline in older adults. *J Alzheimers Dis*. 2017;61:67-78. doi:10.3233/JAD-170658
27. Jung C-R, Lin Y-T, Hwang B-F. Ozone, particulate matter, and newly diagnosed Alzheimer's disease: a population-based cohort study in Taiwan. *J Alzheimers Dis*. 2015;44:573-584. doi:10.3233/JAD-140855
28. Wu Y, Lin Y, Yu H, et al. Association between air pollutants and dementia risk in the elderly. *Alzheimers Dement*. 2015;1:220-228. doi:10.1016/j.dadm.2014.11.015
29. Greve HJ, Dunbar AL, Lombo CG, et al. The bidirectional lung brain-axis of amyloid-β pathology: ozone dysregulates the perivascular microenvironment. *Brain*. 2023;146:991-1005. doi:10.1093/brain/awac113
30. Tyler CR, Noor S, Young TL, et al. Aging exacerbates neuroinflammatory outcomes induced by acute ozone exposure. *Toxicol Sci*. 2018;163:123-139. doi:10.1093/toxsci/kfy014
31. Kodavanti PRS, Valdez M, Richards JE, et al. Ozone-induced changes in oxidative stress parameters in brain regions of adult, middle-age, and senescent Brown Norway rats. *Toxicol Appl Pharmacol*. 2021;410:115351. doi:10.1016/j.taap.2020.115351
32. Akhter H, Ballinger C, Liu N, van Groen T, Postlethwait EM, Liu R-M. Cyclic ozone exposure induces gender-dependent neuropathology and memory decline in an animal model of Alzheimer's disease. *Toxicol Sci*. 2015;147:222-234. doi:10.1093/toxsci/kfv124
33. Avila-Costa MR, Colıń-Barenque L, Fortoul TI, et al. Memory deterioration in an oxidative stress model and its correlation with cytological changes on rat hippocampus CA1. *Neurosci Lett*. 1999;270:107-109. doi:10.1016/S0304-3940(99)00458-9
34. Rivas-Arancibia S, Vazquez-Sandoval R, Gonzalez-Kladiano D, Schneider-Rivas S, Lechuga-Guerrero A. Effects of ozone exposure in rats on memory and levels of brain and pulmonary superoxide dismutase. *Environ Res*. 1998;76:33-39. doi:10.1006/enrs.1997.3784
35. Rivas-Arancibia S, Zimbrón LFH, Rodríguez-Martínez E, Maldonado PD, Borgonio Pérez G, Sepúlveda-Parada M. Oxidative stress-dependent changes in immune responses and cell death in the substantia nigra after ozone exposure in rat. *Front Aging Neurosci*. 2015;7:65. doi:10.3389/fnagi.2015.00065
36. Rodríguez-Martínez E, Martínez F, Espinosa-García MT, Maldonado P. Rivas-Arancibia S. Mitochondrial dysfunction in the hippocampus of rats caused by chronic oxidative stress. *Neuroscience*. 2013;252:384-395. doi:10.1016/j.neuroscience.2013.08.018
37. Rivas-Arancibia S, Hernández-Zimbrón LF, Rodríguez-Martínez E, Borgonio-Pérez G, Velumani V, Durán-Bedolla J. Chronic exposure to low doses of ozone produces a state of oxidative stress and blood-brain barrier damage in the hippocampus of rat. *ABB*. 2013;04:24-29. doi:10.4236/abb.2013.411A2004
38. Frampton MW, Pryor WA, Cueto R, Cox C, Morrow PE, Utell MJ. Ozone exposure increases aldehydes in epithelial lining fluid in human lung. *Am J Respir Crit Care Med*. 1999;159:1134-1137. doi:10.1164/ajrccm.159.4.9807057
39. Pryor WA, Squadrito GL, Friedman M. A new mechanism for the toxicity of ozone. *Toxicol Lett*. 1995;82-83:287-293. doi:10.1016/0378-4274(95)03563-X
40. Pryor WA. How far does ozone penetrate into the pulmonary air/tissue boundary before it reacts? *Free Radical Biol Med*. 1992;12:83-88. doi:10.1016/0891-5849(92)90060-T
41. Mumaw CL, Levesque S, McGraw C, et al. Microglial priming through the lung–brain axis: the role of air pollution–induced circulating factors. *FASEB J*. 2016;30:1880-1891. doi:10.1096/fj.201500047

42. Erickson MA, Jude J, Zhao H, et al. Serum amyloid A: an ozone-induced circulating factor with potentially important functions in the lung-brain axis. *FASEB J*. 2017;31:3950-3965. doi:10.1096/fj.201600857RRR
43. Cheng H, Saffari A, Sioutas C, Forman HJ, Morgan TE, Finch CE. Nanoscale particulate matter from urban traffic rapidly induces oxidative stress and inflammation in olfactory epithelium with concomitant effects on brain. *Environ Health Perspect*. 2016;124:1537-1546. doi:10.1289/EHP134
44. Johnson NF, Hotchkiss JA, Harkema JR, Henderson RF. Proliferative responses of rat nasal epithelia to ozone. *Toxicol Appl Pharmacol*. 1990;103:143-155. doi:10.1016/0041-008X(90)90270-5
45. Hardy J, Allsop D. Amyloid deposition as the central event in the aetiology of Alzheimer's disease. *Trends Pharmacol Sci*. 1991;12:383-388. doi:10.1016/0165-6147(91)90609-V
46. Carter SF, Herholz K, Rosa-Neto P, Pellerin L, Nordberg A, Zimmer ER. Astrocyte biomarkers in Alzheimer's disease. *Trends Mol Med*. 2019;25:77-95. doi:10.1016/j.molmed.2018.11.006
47. Mattsson-Carlgren N, Andersson E, Janelidze S, et al. Aβ deposition is associated with increases in soluble and phosphorylated tau that precede a positive tau PET in Alzheimer's disease. *Sci Adv*. 2020;6:eaaz2387. doi:10.1126/sciadv.aaz2387
48. De Strooper B, Karran E. The cellular phase of Alzheimer's disease. *Cell*. 2016;164:603-615. doi:10.1016/j.cell.2015.12.056
49. Olsen M, Aguilar X, Sehlin D, et al. Astroglial responses to amyloid-beta progression in a mouse model of Alzheimer's disease. *Mol Imaging Biol*. 2018;20:605-614. doi:10.1007/s11307-017-1153-z
50. Keren-Shaul H, Spinrad A, Weiner A, et al. A unique microglia type associated with restricting development of Alzheimer's disease. *Cell*. 2017;169:1276-1290.e17. doi:10.1016/j.cell.2017.05.018
51. Reed-Geaghan EG, Croxford AL, Becher B, Landreth GE. Plaque-associated myeloid cells derive from resident microglia in an Alzheimer's disease model. *J Exp Med*. 2020;217:e20191374. doi:10.1084/jem.20191374
52. Wang Y, Ulland TK, Ulrich JD, et al. TREM2-mediated early microglial response limits diffusion and toxicity of amyloid plaques. *J Exp Med*. 2016;213:667-675. doi:10.1084/jem.20151948
53. Habib N, McCabe C, Medina S, et al. Disease-associated astrocytes in Alzheimer's disease and aging. *Nat Neurosci*. 2020;23:701-706. doi:10.1038/s41593-020-0624-8
54. Liu C-C, Hu J, Zhao N, et al. Astrocytic LRP1 mediates brain Aβ clearance and impacts amyloid deposition. *J Neurosci*. 2017;37:4023-4031. doi:10.1523/JNEUROSCI.3442-16.2017
55. Nielsen HM, Mulder SD, Beliën JAM, Musters RJP, Eikelenboom P, Veerhuis R. Astrocytic Aβ1-42 uptake is determined by Aβ-aggregation state and the presence of amyloid-associated proteins: uptake of Aβ1-42 oligomers and fibrils. *Glia*. 2010;58:1235-1246. doi:10.1002/glia.21004
56. Holmes C, Cunningham C, Zotova E, et al. Systemic inflammation and disease progression in Alzheimer disease. *Neurology*. 2009;73:768-774. doi:10.1212/WNL.0b013e3181b6bb95
57. Thome AD, Faridar A, Beers DR, et al. Functional alterations of myeloid cells during the course of Alzheimer's disease. *Mol Neurodegeneration*. 2018;13:61. doi:10.1186/s13024-018-0293-1
58. Lotze MT, Tracey KJ. High-mobility group box 1 protein (HMGB1): nuclear weapon in the immune arsenal. *Nat Rev Immunol*. 2005;5:331-342. doi:10.1038/nri1594
59. Festoff BW, Sajja RK, van Dreden P, Cucullo L. HMGB1 and thrombin mediate the blood-brain barrier dysfunction acting as biomarkers of neuroinflammation and progression to neurodegeneration in Alzheimer's disease. *J Neuroinflam*. 2016;13:134. doi:10.1186/s12974-016-0670-z
60. Fujita K, Motoki K, Tagawa K, et al. HMGB1, a pathogenic molecule that induces neurite degeneration via TLR4-MARCKS, is a potential therapeutic target for Alzheimer's disease. *Sci Rep*. 2016;6:31895. doi:10.1038/srep31895
61. Oakley H, Cole SL, Logan S, et al. Intraneuronal beta-amyloid aggregates, neurodegeneration, and neuron loss in transgenic mice with five familial Alzheimer's disease mutations: potential factors in amyloid plaque formation. *J Neurosci*. 2006;26:10129-10140. doi:10.1523/JNEUROSCI.1202-06.2006
62. Sadleir KR, Eimer WA, Cole SL, Vassar R. Aβ reduction in BACE1 heterozygous null 5XFAD mice is associated with transgenic APP level. *Mol Neurodegeneration*. 2015;10:1. doi:10.1186/1750-1326-10-1
63. Sadleir KR, Popovic J, Vassar R. ER stress is not elevated in the 5XFAD mouse model of Alzheimer's disease. *J Biol Chem*. 2018;293:18434-18443. doi:10.1074/jbc.RA118.005769
64. Yanai H, Matsuda A, An J, et al. Conditional ablation of HMGB1 in mice reveals its protective function against endotoxemia and bacterial infection. *P Natl Acad Sci USA*. 2013;110:20699-20704. doi:10.1073/pnas.1320808110
65. Hinners RG, Burkart JK, Punte CL. Animal inhalation exposure chambers. archives of environmental health. *An International J*. 1968;16:194-206. doi:10.1080/00039896.1968.10665043
66. Hatch GE, Slade R, Harris LP, et al. Ozone dose and effect in humans and rats. A comparison using oxygen-18 labeling and bronchoalveolar lavage. *Am J Respir Crit Care Med*. 1994;150:676-683. doi:10.1164/ajrccm.150.3.8087337
67. Plopper CG, Hyde DM. The non-human primate as a model for studying COPD and asthma. *Pulm Pharmacol Ther*. 2008;21:755-766. doi:10.1016/j.pupt.2008.01.008
68. Ballinger CA, Cueto R, Squadrito G, et al. Antioxidant-mediated augmentation of ozone-induced membrane oxidation. *Free Radical Biol Med*. 2005;38:515-526. doi:10.1016/j.freeradbiomed.2004.11.009
69. Segura P, Montaño LM, Bazán-Perkins B, Gustin P, Vargas MH. Ozone at high-pollution urban levels causes airway hyperresponsiveness to substance P but not to other agonists. *Environ Toxicol Pharmacol*. 1997;3:91-95. doi:10.1016/S1382-6689(96)00144-5
70. Paxinos G, Franklin KBJ, Franklin KBJ. *The Mouse Brain in Stereotaxic Coordinates*. 2nd ed. Academic Press; 2001.
71. Escartin C, Galea E, Lakatos A, et al. Reactive astrocyte nomenclature, definitions, and future directions. *Nat Neurosci*. 2021;24:312-325. doi:10.1038/s41593-020-00783-4
72. Michalovicz LT, Kelly KA, Vashishtha S, et al. Astrocyte-specific transcriptome analysis using the ALDH1L1 bacTRAP mouse reveals novel biomarkers of astrogliosis in response to neurotoxicity. *J Neurochem*. 2019;150:420-440. doi:10.1111/jnc.14800
73. Mucke L, Yu G-Q, McConlogue L, Rockenstein EM, Abraham CR, Masliah E. Astroglial expression of human α1-antichymotrypsin enhances Alzheimer-like pathology in amyloid protein precursor transgenic mice. *Am J Pathol*. 2000;157:2003-2010. doi:10.1016/S0002-9440(10)64839-0
74. Drobny A, Prieto Huarcaya S, Dobert J, et al. The role of lysosomal cathepsins in neurodegeneration: mechanistic insights, diagnostic potential and therapeutic approaches. *Biochim Biophys Acta Mol Cell Res*. 2022;1869:119243. doi:10.1016/j.bbamcr.2022.119243
75. Dejanovic B, Wu T, Tsai M-C, et al. Complement C1q-dependent excitatory and inhibitory synapse elimination by astrocytes and microglia in Alzheimer's disease mouse models. *Nat Aging*. 2022;2:837-850. doi:10.1038/s43587-022-00281-1
76. Davidson KR, Ha DM, Schwarz MI, Chan ED. Bronchoalveolar lavage as a diagnostic procedure: a review of known cellular and molecular findings in various lung diseases. *J Thorac Dis*. 2020;12:4991-5019. doi:10.21037/jtd-20-651
77. Garza-Lombó C, Thang M, Greve HJ, et al. Circulating HMGB1 is elevated in veterans with Gulf War illness and triggers the persistent pro-inflammatory microglia phenotype in male C57Bl/6J mice. *Transl Psychiatry*. 2021;11:390. doi:10.1038/s41398-021-01517-1

78. Shin S, Bai L, Burnett RT, et al. Air pollution as a risk factor for incident chronic obstructive pulmonary disease and asthma. A 15-year population-based cohort study. *Am J Respir Crit Care Med*. 2021;203:1138-1148. doi:10.1164/rccm.201909-1744OC
79. Thurston GD. Air pollution as an underappreciated cause of asthma symptoms. *JAMA*. 2003;290:1915. doi:10.1001/jama.290.14.1915
80. Nair AK, Van Hulle CA, Bendlin BB, et al. Asthma amplifies dementia risk: evidence from CSF biomarkers and cognitive decline. *A&D Transl Res & Clin Interv*. 2022;8:e12315. doi:10.1002/trc2.12315
81. Wang J, Li X, Lei S, et al. Risk of dementia or cognitive impairment in COPD patients: a meta-analysis of cohort studies. *Front Aging Neurosci*. 2022;14:962562. doi:10.3389/fnagi.2022.962562
82. Rostami J, Mothes T, Kolahdouzan M, et al. Crosstalk between astrocytes and microglia results in increased degradation of α-synuclein and amyloid-β aggregates. *J Neuroinflammation*. 2021;18:124. doi:10.1186/s12974-021-02158-3
83. Erickson MA, Banks WA, Baumann KK. Measurement of blood-brain barrier disruption in mice following ozone exposure using highly sensitive radiotracer assays. *Curr Protoc*. 2022;2:e460. doi:10.1002/cpz1.460
84. Bhalla DK. Ozone-Induced lung inflammation and mucosal barrier disruption: toxicology, mechanisms, and implications. *J Toxicol Environ Health B Crit Rev*. 1999;2:31-86. doi:10.1080/109374099281232

SUPPORTING INFORMATION

Additional supporting information can be found online in the Supporting Information section at the end of this article.

How to cite this article: Ahmed C, Greve HJ, Garza-Lombo C, et al. Peripheral HMGB1 is linked to O_3 pathology of disease-associated astrocytes and amyloid. *Alzheimer's Dement*. 2024;20:3551–3566. https://doi.org/10.1002/alz.13825